Understanding the Drivers of Atlantic Multidecadal Variability Using a Stochastic Model Hierarchy

GLENN LIU,[a] YOUNG-OH KWON,[b] CLAUDE FRANKIGNOUL,[b,c] AND JIAN LU[d]

[a] *Massachusetts Institute of Technology–Woods Hole Oceanographic Institution Joint Program, Woods Hole, Massachusetts*
[b] *Woods Hole Oceanographic Institution, Woods Hole, Massachusetts*
[c] *LOCEAN, Sorbonne Université/IRD/CNRS/MNHN, Paris, France*
[d] *Pacific Northwest National Laboratory, Richland, Washington*

(Manuscript received 27 April 2022, in final form 26 August 2022)

ABSTRACT: The relative importance of ocean and atmospheric dynamics in generating Atlantic multidecadal variability (AMV) remains an open question. Comparisons between climate models with a slab ocean (SLAB) and fully dynamic ocean components (FULL) are often used to explore this question, but cannot reveal how individual ocean processes generate these differences. We build a hierarchy of physically interpretable stochastic models to investigate the contribution of two upper-ocean processes to AMV: the role of seasonal variation and mixed-layer entrainment. This interpretability arises from the stochastic model's simplified representation of sea surface temperature (SST), considering only the local upper-ocean response to white-noise atmospheric forcing and its impact on surface heat exchange. We focus on understanding differences between SLAB and FULL non-eddy-resolving preindustrial control simulations of the Community Earth System Model 1 (CESM), and estimate the stochastic model parameters from each respective simulation. Despite its simplicity, the stochastic model reproduces temporal characteristics of SST variability in the SPG, including reemergence, seasonal-to-interannual persistence, and power spectra. Furthermore, the unrealistically persistent SST of the CESM-SLAB ocean simulation is reproduced in the equivalent stochastic model configuration where the mixed-layer depth (MLD) is constant. The stochastic model also reveals that vertical entrainment primarily damps SST variability, thus explaining why SLAB exhibits larger SST variance than FULL. The stochastic model driven by temporally stochastic, spatially coherent forcing patterns reproduces the canonical AMV pattern. However, the amplitude of low-frequency variability remains underestimated, suggesting a role for ocean dynamics beyond entrainment.

KEYWORDS: North Atlantic Ocean; Atmosphere-ocean interaction; Oceanic mixed layer; Stochastic models; Climate variability; Multidecadal variability

1. Introduction

Understanding the ocean's "memory" and mechanisms controlling the persistence of large-scale sea surface temperature (SST) anomalies is critical for the prediction of interannual and multidecadal climate variability. The idea of memory stems from the ocean's large thermal inertia: rapidly varying atmospheric conditions are communicated via surface fluxes into the ocean, where they are integrated into slowly varying SSTs. This partitioning of the atmosphere–ocean system into two time scales was first utilized by Hasselmann (1976) in his stochastic model for climate variability. Its subsequent application to modeling the response of mixed-layer temperatures to white-noise atmospheric forcing and empirically estimated damping successfully replicated the magnitude and spectral characteristics of midlatitude SST anomalies up to interannual time scales (Frankignoul and Hasselmann 1977, hereafter FH77). Atmospheric forcing of SSTs at these time scales is generally dominated by surface heat fluxes, but mixed-layer depth (MLD) variability and, in regions of large SST gradients, Ekman currents may also play a role in driving SST anomalies. These anomalies are largely damped by surface heat flux feedback and entrainment (Frankignoul 1985; Alexander and Penland 1996).

At decadal and longer time scales, the relative importance of atmosphere versus ocean dynamics for SST variability remains uncertain. In the North Atlantic region, the debate surrounds identifying the key driver of the Atlantic multidecadal variability (AMV; or the Atlantic multidecadal oscillation). AMV describes the basinwide fluctuation of SST anomalies with maximum loading in the subpolar gyre (SPG) (Deser et al. 2010). Despite its numerous impacts across the climate system, including Atlantic hurricane activity, extreme temperatures, and precipitation over the surrounding continents, regime shifts in Atlantic fish populations, and even conditions in the Pacific Ocean, there is little consensus on AMV's primary driver (Gao et al. 2019; Zhang and Delworth 2006; Alheit et al. 2014; Meehl et al. 2021).

One viewpoint is that the AMV is primarily driven by ocean dynamics, especially by the changes in the Atlantic meridional overturning circulation (AMOC) that affect the poleward transport of heat (Knight et al. 2005; Kim et al. 2018b; Zhang et al. 2019). This was challenged by Clement et al. (2015), who found that slab ocean simulations (hereafter SLAB), with no active ocean dynamics, reproduce both spatial and spectral characteristics of AMV consistent with models containing full ocean dynamics (hereafter FULL). They suggested that AMV is instead predominantly driven by changes in surface heat flux forcing stemming from internal atmospheric variability, such

Denotes content that is immediately available upon publication as open access.

Corresponding author: Glenn Liu, glennliu@mit.edu

DOI: 10.1175/JCLI-D-22-0309.1

as the North Atlantic Oscillation (NAO). This ignited a vigorous debate on the extent to which ocean dynamics are necessary for AMV (Zhang et al. 2016; O'Reilly et al. 2016; Li et al. 2020). Most recently, studies have found greater SST variance in SLAB simulations, particularly at multidecadal frequencies, indicating that ocean dynamics primarily act to damp low-frequency SST variability (Murphy et al. 2021; Patrizio and Thompson 2022).

The simplicity of the SLAB approach is its primary limitation: complete exclusion of interactive ocean dynamics obscures deeper understanding of how individual processes contribute to SST variability and create differences between SLAB versus FULL simulations. To address this, we developed a hierarchy of stochastic models with increasingly complex representations of heat flux feedback, atmospheric forcing, and mixed-layer behavior, while still neglecting oceanic advection. These processes are known to exhibit seasonal modulations, and we apply the stochastic model to systematically investigate their contributions to low-frequency Atlantic SST variability (Ortiz and De Elvira 1985; Alexander and Penland 1996; Park et al. 2006).

In the absence of ocean circulation, vertical entrainment of SST anomalies from below the seasonal mixed layer provides a potential pathway for anomalies to persist to lower frequencies. Specifically, anomalies formed in the deep winter mixed layer are insulated and preserved beneath the shallow summer thermocline. As the mixed layer deepens during the following fall and winter, the anomaly is re-entrained into the surface layers, impacting conditions the following year (Alexander and Deser 1995). Previous studies including the entrainment term in the stochastic model recovered the 1–3-yr wintertime re-emergence of both the NAO-related tripole pattern of SST anomalies and area-averaged conditions over the North Pacific and Atlantic (de Coëtlogon and Frankignoul 2003; Deser et al. 2003; Park et al. 2006; Li et al. 2020). In contrast to the interannual re-emergence of large-scale SST patterns, pointwise heat budget analyses have suggested that vertical entrainment primarily damps low-frequency SSTs (Yamamoto et al. 2020; Patrizio and Thompson 2021). Thus, the competing contributions of re-emergence versus damping associated with vertical entrainment to multidecadal SST variability remain unclear. Application of the stochastic model hierarchy at individual locations across the North Atlantic provides an opportunity to investigate this competing effect across time scales and from *both* local and regionally averaged perspectives without the influence of additional ocean dynamics.

Efforts to determine the ocean's role in the internal component of AMV since Clement et al. (2015), particularly those applying the stochastic model, have predominantly focused on the *temporal* aspects of SST variability rather than the origins of the *spatial pattern* of AMV. We revisit this aspect, using the stochastic model to investigate how the local mixed-layer response to stochastic forcing corresponding to dominant atmospheric modes can reproduce AMV-like patterns without interactive ocean dynamics. The role of the latter is inferred by comparison with a fully coupled simulation.

In summary, we strive to address the following questions using the stochastic model hierarchy to understand SST and AMV behavior in the SLAB and FULL Community Earth System Model version 1 (CESM1) simulations:

1) How does seasonal variation in upper-ocean processes and atmospheric forcing influence SST variability?
2) What role do entrainment and other ocean dynamics play in shaping the spatiotemporal characteristics of AMV?
3) Can spatially coherent structure in temporally random atmospheric forcing reproduce the canonical AMV pattern in the stochastic model?

The structure of this paper is as follows. We first present the CESM1 model simulations used for our analyses (section 2), then introduce the stochastic models and hierarchical approach (section 3). The estimation of stochastic model parameters is detailed (section 4). We then examine a case study in the SPG to understand how seasonal variation of the atmospheric forcing and upper-ocean parameters impact SST behavior in CESM1 (section 5a). The analysis is repeated on regionally averaged output to assess the generalizability of our conclusions (section 5b), and the model's ability to reproduce the CESM1 AMV pattern is presented (section 5c). A discussion and summary are provided in sections 6 and 7.

2. Data

Community Earth System Model version 1 simulations

The limited observational record presents a major challenge to understanding SST variability, particularly low-frequency phenomena such as the AMV. Long climate model simulations can instead provide a larger subsampling of SST behavior. We use CESM1, a fully coupled general circulation model with land, ice, atmosphere, and ocean components all of nominally 1° horizontal resolution (Hurrell et al. 2013). The preindustrial control experiment featuring aerosol and radiative forcing fixed at 1850 levels is used to investigate natural variability of the climate system without changes in external forcing. We use years 400–2200 in the analysis to avoid contributions from initialization.

In addition to the fully coupled configuration (CESM-FULL), we analyze the slab ocean simulation (CESM-SLAB). CESM-SLAB has identical configurations to CESM-FULL except that the ocean component is a slab ocean model subject only to air–sea heat fluxes and a prescribed flux correction with no interactive lateral or vertical ocean processes. The thickness of the slab at each location is set to the annual mean boundary layer depth from the climatological cycle of CESM-FULL, thus *spatially varying but temporally constant* (He et al. 2017). MLDs in CESM1 are determined using a maximum buoyancy gradient criterion (Smith et al. 2010). The climatological monthly flux correction term for CESM-SLAB is diagnosed from CESM-FULL, representing the mean heat convergence and divergence induced by ocean dynamics needed to maintain a realistic SST climatology (Bitz et al. 2012). CESM-SLAB provides an opportunity to study SST behavior considering only the local, upper-ocean response to atmospheric forcing, dependent only upon the thermal capacity of the slab ocean. Monthly output from years 200 to 1100 is used in the analysis.

Prior to our analysis, the mean annual cycle is removed from each simulation to compute the monthly anomalies. We exclude grid points where the sea ice coverage exceeds 5% anytime during the simulation to focus on ocean–atmosphere interactions.

3. Stochastic model

a. Formulation

We begin with a simplified equation for the vertically integrated temperature anomaly (T') over a mixed layer of uniform density, temperature, and horizontal velocities (Frankignoul 1985):

$$\frac{dT'}{dt} = \underbrace{\frac{Q'_{\mathrm{net}}}{\rho C_p \overline{h}}}_{A} - \underbrace{\frac{(h\upsilon)' \cdot \nabla(\overline{T}+T')}{\overline{h}}}_{B} - \underbrace{\frac{h'}{\overline{h}}\frac{\partial \overline{T}}{\partial t}}_{C} - \underbrace{\frac{(T'-T_d')(\overline{w}_e+w_e')}{\overline{h}}}_{D} - \underbrace{\frac{\overline{T}-\overline{T}_d}{\overline{h}} w_e'}_{E} + \underbrace{\kappa\nabla^2 T'}_{F} \qquad (1)$$

where the overbars and primes represent monthly climatological means and monthly anomalies, respectively. The right-hand terms are, in order:

- A: Net heat flux into the mixed layer (Q'_{net}), with the MLD (h), density ($\rho = 1026$ kg m^{-3}), and specific heat ($C_p = 3996$ J kg^{-1} °C^{-1}) of seawater
- B: Advection of the SST gradient by anomalous currents (υ')
- C: Thermal capacity change solely due to MLD anomalies (h')
- D: Entrainment [$w_e = (dh/dt)$] of temperature anomalies from below the mixed-layer (T_d'), nonzero only when the mixed-layer is deepening ($w_e > 0$).
- E: Anomalous entrainment velocity (w_e') acting on mean vertical temperature gradient
- F: Horizontal mixing and eddy stirring, with the horizontal diffusivity (κ)

Equation (1) includes both local and nonlocal ocean dynamics. The variability in large-scale geostrophic currents impacts low-frequency SST variability, and its contribution, along with other nonlocal oceanic components, will be inferred from comparison with CESM-FULL (Frankignoul et al. 1998). To retain the SST characteristics primarily dependent on local atmospheric variability we neglect the term F and the geostrophic advection in term B. We neglect the remainder of term B, including the Ekman component that is small away from regions of large SST gradients. The potential contributions of Ekman advection are explored in section 6c. We additionally neglect terms C and E, and anomalous entrainment velocity in term D. These terms are challenging to represent analytically, but could be approximated as part of the stochastic atmospheric forcing since anomalies in MLD and entrainment are primarily driven by short time scale wind and heat flux variability (Frankignoul 1985; Alexander and Penland 1996; Frankignoul et al. 1998).

A final assumption applies the two-time scale stochastic model framework and neglects vertical mixing at the mixed-layer base and solar radiation absorbed below it. Note that Q'_{net} in term A is expressed as

$$Q'_{\mathrm{net}} = -\lambda_a T' + F'. \qquad (2)$$

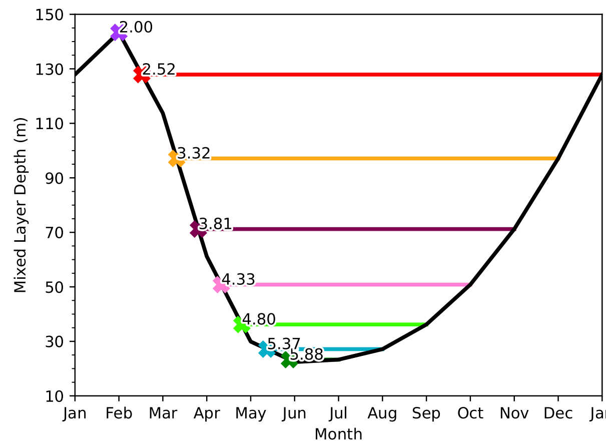

FIG. 1. Example calculation of T_d' for the seasonal mixed-layer cycle (black line) at a subpolar test point (50°N, 30°W). The labeled detrainment times (months, where 1 = January), indicated by ×, are connected to the corresponding entrainment month by the colored line. T_d' is calculated by linearly interpolating between temperature values for the nearest months around the detrainment time.

The key assumption is that the local Q'_{net} into the ocean can be decomposed into a component linearly dependent on T' and a stochastic forcing (F') independent of the local SST anomalies where λ_a is the strength of atmospheric heat flux feedback (Frankignoul et al. 1998). The result of all these assumptions is the stochastic model equation:

$$\frac{\partial T'}{\partial t} = -\frac{\lambda_a}{\rho C_p h} T' + \frac{F'}{\rho C_p h} - \frac{1}{h}\overline{w}_e (T' - T_d'), \qquad (3)$$

where T' is the temperature anomaly vertically averaged through the mean monthly mixed layer ($\overline{h}$ is hereafter h).

From this analytical form, the equation is further simplified by combining entrainment and atmospheric damping [$\lambda = (\lambda_a/\rho C_p h) + (\overline{w_e}/h)$]. Equation (3) is integrated with the forward method at a monthly step from t to $t + \Delta t$ to yield

$$T'(t+\Delta t) = e^{-\lambda \Delta t} T'(t) + \int_t^{t+\Delta t} \left[\frac{F'}{\rho c_p h} + \left(\frac{\overline{w_e}}{h}\right) T_d'\right] e^{-\lambda\,(t+\Delta t - t')} dt'. \qquad (4)$$

The temperature anomaly below the mixed layer (T_d') is computed during the integration using T' from the prior detrainment at the same depth (Fig. 1). Note that T_d' is determined through linear interpolation, and is averaged over the monthly time step:

$$(\overline{T_d'}) = \frac{T_d'(t) + T_d'(t+\Delta t)}{2}. \qquad (5)$$

Assuming the parameters [$(\overline{\lambda}_a/\rho C_p h)$, $(\overline{w}_e/h)$, $(\overline{F'}/\rho C_p h)$, $(\overline{T_d'})$] are constant over the monthly time step (Δt), the integral in Eq. (4) is evaluated to yield

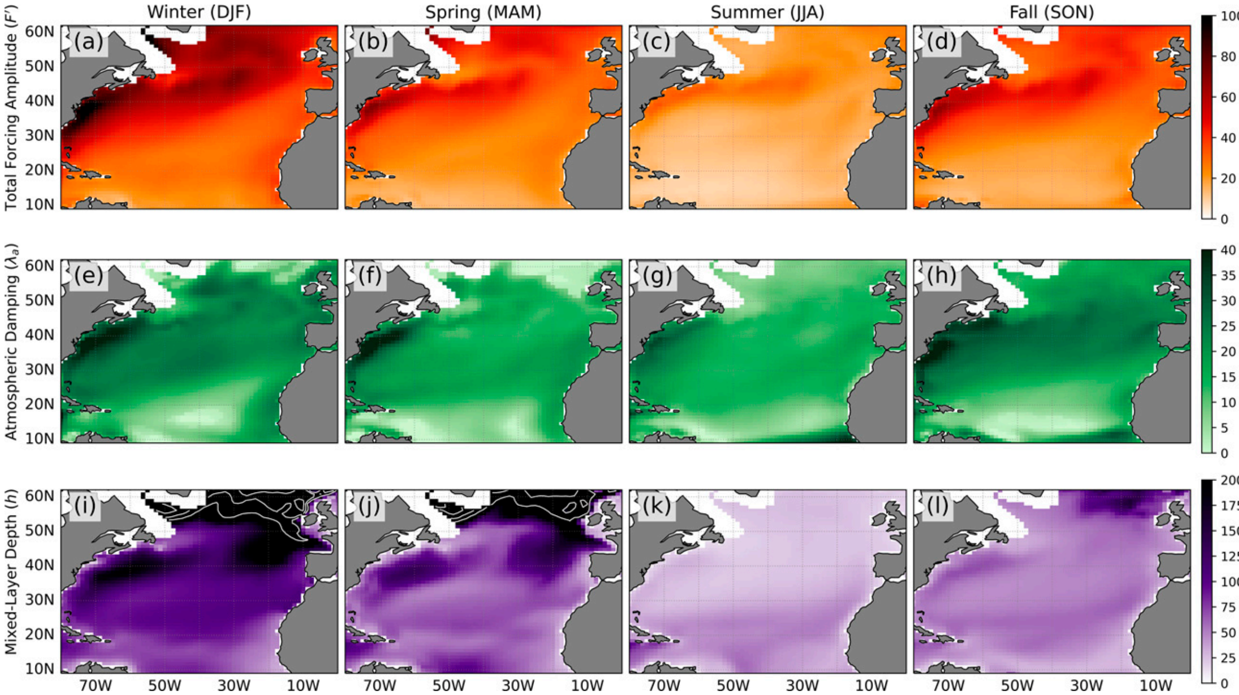

FIG. 2. Seasonal mean estimates for (left to right) winter to fall of (a)–(d) stochastic forcing amplitude (in W m^{-2}), (e)–(h) atmospheric heat flux feedback strength (in W m^{-2} °C^{-1}), and (i)–(l) MLD (in m) from CESM-FULL, where depths greater than 300 m are contoured every 150 m. Note that we force the stochastic model with monthly varying values; seasonal averages are shown here for illustration.

$$T'(t+\Delta t) = e^{-\lambda\Delta t}\,T'(t) + \left\{\frac{1}{\Delta t}\ln\left[\frac{h(t+\Delta t)}{h(t)}\right]\overline{T'_d} + \left(\frac{F'}{\rho C_p h}\right)\right\}\left(\frac{1-e^{-\lambda\Delta t}}{\lambda}\right). \quad (6)$$

The stochastic model requires only three seasonally varying input parameters: the atmospheric heat flux feedback strength (λ_a), the amplitude of stochastic forcing (F'), and MLD (h). The latter is obtained from the climatological mean monthly MLD cycle from CESM-FULL (Figs. 2i–l). Note that h is shallow (<100 m) in the summer and deepest in the subpolar region during the winter and spring.

b. *Model hierarchy*

We build a hierarchy of stochastic models by successively adding seasonal variation into λ_a, F', and h and examining their impact on SST variability (Fig. 3a). The hierarchy is divided into two sections. In the lower, non-entraining section ($w_e = 0$; Levels 1–3), we investigate the effect of including seasonal variation in λ_a and F'. This begins with the canonical stochastic model first proposed by FH77, or Eq. (3) with the entrainment term omitted (Fig. 3; Level 1). Seasonal variation in λ_a (Level 2a) or F' (Level 2b) is introduced individually (Level 2). As the closest analogy to the slab ocean configuration, the case with seasonal variation in *both* λ_a and F', but constant h (Level 3) is compared to CESM-SLAB.

In the upper section (Levels 4–5), we investigate the effect of increasing MLD complexity. First, seasonal variation in h is included (Level 4), followed by the entrainment term (Level 5; $w_e \neq 0$). The entraining stochastic model is compared with CESM-FULL to infer the role of ocean dynamics beyond entrainment.

4. Parameter estimation

a. *Estimating heat flux feedback*

An important step for separating atmospheric and oceanic controls on SST variability lies in carefully distinguishing their contributions to damping SST anomalies. We define the *atmospheric* heat flux feedback (λ_a) as the Q'_{net} (into the atmosphere) induced by a given SST anomaly (T') [see Eq. (2)]. To directly estimate λ_a, we employ a statistical method that uses Q'_{net} and T' from CESM-FULL or CESM-SLAB (Frankignoul and Kestenare 2002, hereafter FK2002). Since Q'_{net} includes both radiative and turbulent components of the surface flux, the estimated damping includes radiative feedbacks (Park et al. 2005). Taking the lagged covariance of Eq. (2) with T' with a lag longer than the typical persistence of atmospheric internal noise causes the forcing term (F') to vanish (FK2002). Then λ_a (W m^2 °C^{-1}) can be statistically estimated from the ratio between the remaining two terms as

$$\lambda_a = -\frac{\text{cov}[T'(t-\tau), Q'_{net}(t)]}{\text{cov}[T'(t-\tau), T'(t)]}, \quad (7)$$

where τ is the lag in months. The term λ_a is computed separately at each spatial point in the North Atlantic for $\tau = 1$ month. We

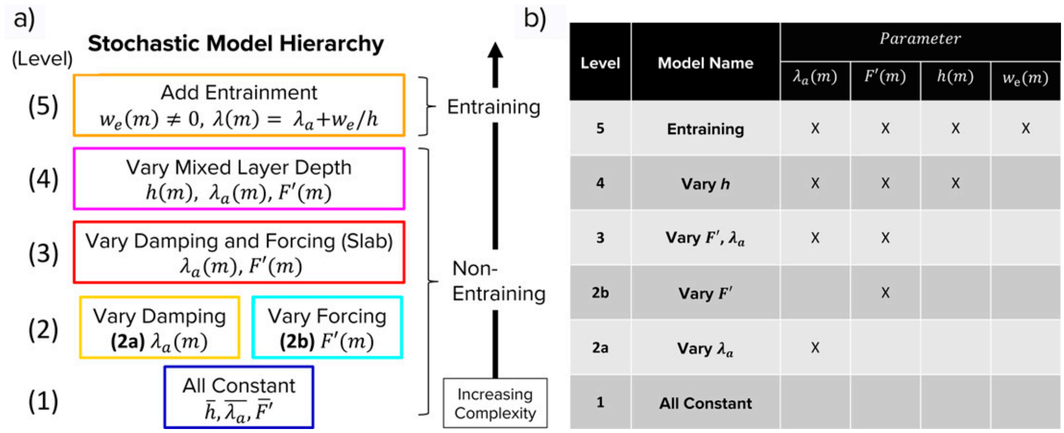

FIG. 3. (a) Stochastic model hierarchy, increasing in complexity from bottom to top; h, λ_a, and F' indicate the MLD, atmospheric heat flux feedback strength, and amplitude of stochastic forcing, respectively. Overbars indicate annual mean values, while m indicates climatological monthly variation. In the entraining model, additional damping from the entrainment (w_e) is included. (b) The same information is summarized in a table, where × denotes that seasonal variation in the corresponding variable is included.

assess the statistical significance of our estimates using a two-sided Student's t test at a 5% significance level (Park et al. 2005). The value of λ_a is set to zero when and where the covariance in either the numerator or denominator is statistically insignificant. Insignificant estimates with weakly positive or near-zero covariances occurred over the western tropics and high-latitude northeastern Atlantic in CESM-FULL, leading to unrealistically large SST variances in the stochastic models. We replaced these values with corresponding estimates from CESM-SLAB and *focused our analyses on extratropical points between 20° to 60°N* (see sections 4c and 6c). Insignificant regions are marked when presenting the AMV patterns (e.g., Fig. 8b).

A potential source of longer (greater than multiple weeks) atmospheric memory is remote forcing, such as from El Niño–Southern Oscillation (ENSO). To reduce bias due to this persistent source, we first compute the ENSO-related components of heat flux and SSTs, then remove those components prior to estimating λ_a (FK2002; Park et al. 2005). ENSO indices are defined based on the two leading empirical orthogonal functions (EOFs) of the tropical Pacific SST, representative of the central and eastern modes (20°S–20°N, 120°–240°E). The heat flux and SST in the North Atlantic are then regressed on the ENSO indices to get the ENSO-related components, which are subsequently subtracted from the full anomalies of both fields. *ENSO was only removed for estimating λ_a, and is retained for all other analyses in this paper*.

The separation of λ_a and entrainment damping contrasts with previous work using the stochastic model that estimated an overall damping (λ) using an exponential fit to the SST autocorrelation, an approach that conflates contributions from both atmospheric and oceanic damping (FH77; de Coëtlogon and Frankignoul 2003; Deser et al. 2003). Our approach provides an opportunity to investigate if these previous works overestimated (underestimated) damping due to the atmosphere (ocean), and to further discern how each component impacts the SST persistence.

Our estimates of λ_a from CESM1 agree with previous work based on observations that reported values between 10 and 35 W m^{-2} °C^{-1}, sometimes exceeding 50 W m^{-2} °C^{-1} (Figs. 2e–h) (FK2002; Park et al. 2005). The maxima occur along the Gulf Stream, where cold continental winds cause turbulent heat loss from the warmer ocean during the boreal winter, and are stronger than the maximum reported by Park et al. (2005).

b. *Estimating atmospheric forcing*

Previous estimates of the amplitude of stochastic forcing were based on the local or box-averaged variance of residual heat fluxes after removing the components linearly dependent on SST (e.g., Li et al. 2020). However, this approach does not capture spatial coherence in the forcing pattern, such as opposite-signed relationships in heat flux anomalies between the subtropics and subpolar regions associated with the NAO (Cayan 1992). To retain spatial coherence, we estimate the atmospheric forcing pattern (F') in Eq. (3) using EOFs, and express it in the form

$$F'(x, y, t) = \sum_{n=1}^{k} \alpha(x, y, n, m)\, N_{(0,1)}(n, t), \tag{8}$$

where α is the spatially varying amplitude of stochastic forcing for a given mode n and month m. The term $N_{(0,1)}$ is the corresponding random time series for each mode drawn from a standardized Gaussian distribution.

More specifically, we estimate F' using following steps:

1) The stochastic component of $Q'_{\rm net}$ in CESM1 is computed at each grid point using our estimated heat flux feedback ($F' = Q'_{\rm net} + \lambda_a T$).
2) The spatial pattern of forcing (α) is determined using EOF analysis of F' across the North Atlantic domain (0°–65°N, 80°W–20°E) for each calendar month. The resultant EOFs (in W m^{-2}) are the 12 monthly patterns for each mode (n).

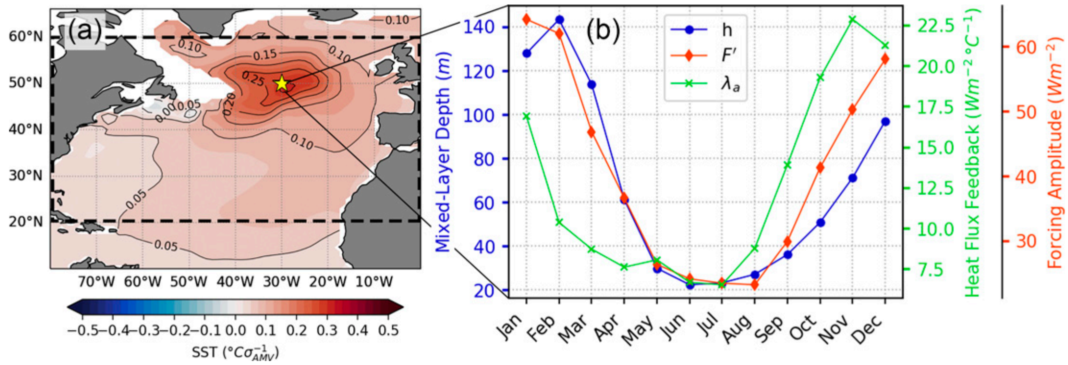

FIG. 4. (a) The AMV SST pattern calculated from the CESM-FULL simulation from 20°–60°N, 80°–0°W (dashed box). The yellow star indicates the location of the subpolar gyre (SPG) point for the case study. (b) Seasonal cycles of inputs parameters for the stochastic model at the SPG point, including MLD (blue; from CESM-FULL) as well as the stochastic forcing amplitude (red) and atmospheric heat flux feedback strength (green; both estimated from CESM-SLAB).

3) For each mode, a white noise time series is generated for the length of the simulation (t = 12 × the number of years) and is multiplied by the corresponding amplitude for each month from the EOF pattern. This creates forcing patterns with seasonally varying magnitude that are coherent in space, but stochastic in time.
4) We retain enough modes to explain 90% of the variance for each month and sum the values to reconstruct the monthly varying forcing at each grid point while filtering out small-scale structures. We then amplify the local white noise to boost the variance of stochastic forcing back to 100% of the total variance to ensure the local amplitude of the forcing is replicated. The resultant forcing exhibits larger amplitudes in winter and spring, particularly along the Gulf Stream and Flemish Cap (Figs. 2a–d).

In summary, this formulation of stochastic forcing allows for explicit examination of how spatial structure and seasonal dependence of F' influence SST variability.

c. Omission of the tropics

The tropics (points equatorward of 20°N) are where two key assumptions for the stochastic model are not appropriate. The first assumption is that the surface heat flux, in particular the solar radiation, is evenly distributed through the mixed layer. This is less valid in the tropics, where the mixed layer is often very shallow and penetration of solar radiation below the mixed-layer base is needed to prevent unrealistically large SST amplitudes (Davis et al. 1981; Hosoda et al. 2016).

The second assumption that atmospheric memory is short relative to the ocean is inappropriate; tropical atmospheric waves and convectively driven fluctuations may have larger persistence than midlatitude synoptic fluctuations, in addition to the influence of remote ENSO forcing (FK2002). Despite ENSO removal, the heat flux feedback estimates in the tropics were weak and insignificant at the 5% level (section 4a), resulting in large SSTs in the stochastic model. This suggests that the sources of tropical atmospheric persistence were insufficiently removed, leading to reduction or cancellation of lag covariance between Q_{net} and SST. Considering these complications, *we omitted points south of 20°N in our regional analyses and AMV index to instead focus our discussion on the extratropics where the stochastic model assumptions hold.*

5. Results from stochastic model integrations

a. A case study in the SPG (50°N, 30°W)

To crystallize our understanding of how seasonal variation and entrainment impact SST variability across time scales, it is useful to first focus on a single location. We thus perform a case study at a point within the SPG (50°N, 30°W; Fig. 4a) selected for three primary reasons:

1) The seasonal cycle is typical of the extratropics for all parameters, with maximum (minimum) values in the winter (summer) (Fig. 4b).
2) The point is away from regions of strong advection, such as the Gulf Stream and the SPG boundary current, allowing for focused analysis on the interplay between the three model parameters and entrainment without confounding variables.
3) Most importantly, it is at the region of maximum loading for the CESM-FULL AMV pattern, providing an opportunity to investigate if the processes included in the stochastic model are adequate to produce realistic low-frequency SST variability where the signal is strongest.

At the point, we integrate the stochastic model *starting from January* at a monthly step for 10 000 years at each level of the hierarchy. We then examine two aspects to capture how seasonal variation of parameters and entrainment impacts SST variability across time scales:

1) Seasonal-to-interannual persistence of SST using the monthly lagged autocorrelation where lag 0 is February, the month of the deepest MLD. This allows for evaluation of an end-member case where we expect persistence to be longest and facilitates detection of the re-emergence signal (Deser et al. 2003).

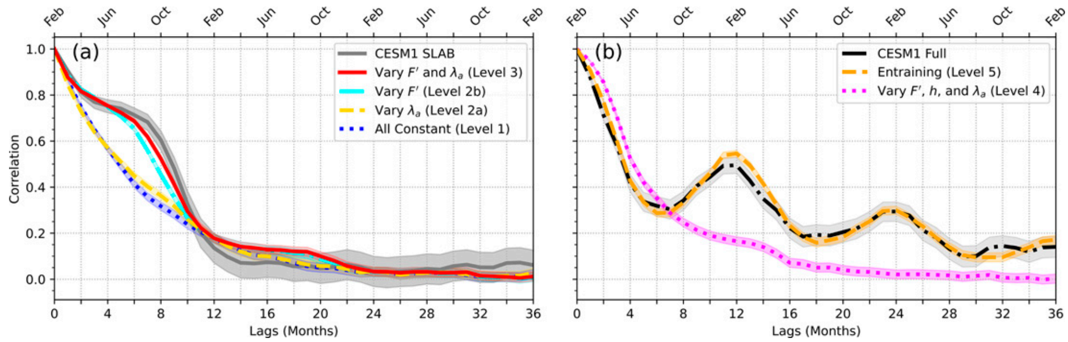

FIG. 5. (a) SST autocorrelations for the stochastic model at the SPG point with a constant MLD of 54.6 m (consistent with CESM-SLAB) including cases where all parameters are constant (Level 1; blue); seasonal variation only in damping (Level 2a; gold) or forcing (Level 2b; cyan); seasonal variation in both (Level 3; red), and CESM-SLAB (gray) for comparison. The shading indicates the 95% confidence level for each correlation. (b) Autocorrelation for the stochastic models with increasing MLD complexity including seasonally varying MLD (Level 4; magenta), and with entrainment (Level 5; orange). For comparison, CESM-FULL (black) is also included.

2) SST power spectra to examine variability at interannual-to-multidecadal time scales, with a focus on lower frequencies to understand the drivers of AMV.

1) Seasonal variation in forcing and damping

The simplest stochastic model with annually averaged parameters (Level 1 All Constant) produces exponentially decaying SST anomalies (blue line, Fig. 5a), a canonical behavior of the FH77 model. In contrast, autocorrelation at the same point in CESM-SLAB (gray line) exhibits slower decorrelation from April to October. This persistent "shoulder" feature is generated by the weaker stochastic forcing during summer while the heat capacity of the mixed-layer remains fixed due to the constant MLD, and is indeed seen in the stochastic model when the seasonal modulation of the stochastic forcing is included [Level 2b Vary F' (cyan) and Level 3 Vary F', λ_a (red lines)]. The inclusion of weaker summertime damping alone does not reproduce this feature (Level 2a Vary λ_a; yellow line), suggesting that seasonal variation in damping is secondary to that of forcing in driving seasonal-to-interannual SST persistence.

Proceeding to longer time scales, all non-entraining stochastic models (Levels 1–4) have SST spectra that broadly resemble first-order autoregressive (AR1) processes without pronounced spectral peaks (Fig. 6a, and magenta curve in Fig. 6b). Adding seasonal variation in damping and forcing slightly increases the overall SST variance, particularly at frequencies between 5 and 20 years (Fig. 6a; Levels 2–3). This frequency dependence suggests that increased summertime persistence in slab-like configurations enhance SST variance beyond seasonal time scales. An important difference between the CESM-SLAB and the stochastic models is that the former includes two-way and nonlocal air–sea interactions, such as the thermally coupled Walker mode described by Clement et al. (2011). These nonlocal processes may provide additional remote forcing, creating larger deviations of the CESM-SLAB spectrum from the AR(1) model. Nevertheless, the total variances for the CESM-SLAB and the stochastic models with fixed MLD are broadly comparable (see the legend of Fig. 6a).

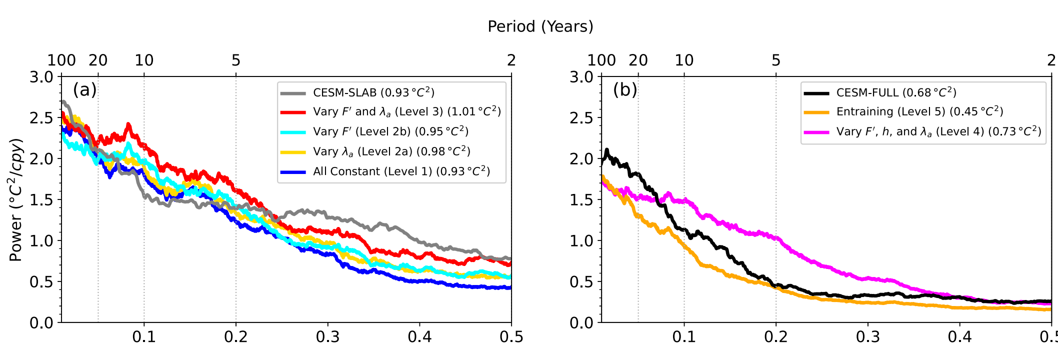

FIG. 6. The SST power spectra at the SPG point for stochastic models for the hierarchy (a) Levels 1–3 (i.e., the non-entraining stochastic models with fixed MLD) and (b) Levels 4–5. The total SST variance for each case is indicated in the legend. Each spectral estimate was tapered by 10%, and smoothed with a modified Daniell window of 350 (stochastic model) or 100 (CESM) adjacent bands.

2) Seasonal mixed-layer depth cycle and entrainment

The importance of seasonal MLD variations is underscored by the disappearance of the summertime persistence with its inclusion (Level 4 Vary h; magenta line, Fig. 5b). Reduced heat capacity due to the shallow summer mixed-layer amplifies both stochastic forcing and heat flux feedback, more than compensating the weaker summertime values of these parameters and acting overall to reduce persistence [see Eqs. (3) and (6)]. This compensation is absent in slab ocean configurations with temporally fixed MLDs, allowing wintertime SST anomalies to persist more readily from year to year, with minimal interruption from weak summertime stochastic forcing. This is further reflected in a large reduction in SST variance at low frequencies when including seasonal MLD variations [Level 4 Vary h (magenta) versus Level 3 Vary F', λ_a (red), Figs. 6a,b].

CESM-FULL exhibits strong rebounds of the autocorrelation in each subsequent winter (black line in Fig. 5b), due to the winter-to-winter re-emergence present in much of the global oceans (Alexander and Deser 1995; Byju et al. 2018). The addition of the entrainment term allows the stochastic model to simulate both the correct timing and amplitude of the re-emergence signal, despite lacking a fully dynamic ocean (Level 5 Entraining; orange vs black lines in Fig. 5b). This suggests that at this location where the CESM-FULL AMV signal is largest, entrainment and seasonal MLD variations are key determinants of SST persistence at seasonal-to-interannual time scales, without the need for additional ocean dynamics.

On interannual and longer time scales, only the inclusion of entrainment alters the shape of the SST spectra by reducing its power, improving agreement with the CESM-FULL. This primarily arises from the entrainment-related damping of SST variability at all frequencies, particularly at interannual time scales [Level 4 Vary h (magenta) versus Level 5 Entraining (orange); Fig. 6b]. However, the SST spectrum is now underestimated at low frequencies compared to CESM-FULL, suggesting that ocean processes beyond vertical entrainment are necessary to enhance low-frequency SST variance (Garuba et al. 2018). Overall, the striking consistency between the short-time scale persistence and the SST spectra at periods up to 5 years of the entraining stochastic model and CESM-FULL lends confidence to the use of the stochastic model for understanding the mechanistic underpinnings of SST variability at this location.

b. *Regional SST analysis*

While seasonal MLD variation and entrainment are important processes for realistic representation of SST variability at the SPG point, their applicability over the broader North Atlantic requires further investigation. We expand our analysis by integrating the model for 10 000 years at each point across the Atlantic basin. Parameters estimated at each grid from the CESM-FULL (SLAB) are used for the entraining (non-entraining) stochastic model to facilitate comparison. The same set of white noise time series is used for all integrations, such that the resultant SSTs are driven by spatially coherent stochastic forcing.

We focus our analysis on three key regions of the AMV horseshoe pattern to examine their dynamical origins: the SPG maximum (40°–65°N, 60°–20°W), subtropical gyre minimum (STGw; 20°–40°N, 80°–40°W), and the lobe of elevated values to the east (STGe; 20°–40°N, 40°–10°W,) (Fig. 7a, inset). Autocorrelations and power spectra are computed from the area-weighted average SST over each region to assess if our conclusions apply beyond our test point. While this box-averaged approach undoubtedly conflates regions with very different dynamics, such as the Gulf Stream and subtropical gyre within STGw, our objective here is to obtain a broader understanding of how entrainment may contribute to subsections of the AMV pattern and large-scale, low-frequency SST behavior.

The conclusions at our test point hold for simulated SSTs averaged over the larger SPG domain; entrainment damps SST variability, particularly at interannual-to-decadal frequencies, and its inclusion allows the stochastic model to approximate the SST autocorrelation in CESM-FULL (Figs. 7a,d). One notable difference is that entrainment enhances SPG-averaged SST variability at time scales greater than 20 years [Fig. 7d, Level 5 Entraining (orange) vs Level 4 Vary h (magenta lines)]. This suggests that at a regional scale, the reddening of the spectrum due to longer memory from re-emergence overpowers the entrainment-related damping. Despite this enhancement, the stochastic model's continued underestimation of the CESM-FULL spectra at low frequencies underscores the importance of low-frequency ocean dynamics beyond entrainment.

Within STGw, damping associated with entrainment yields only modest improvements in modeling the CESM-FULL SST behavior at interannual time scales (Figs. 7b,e). At longer time scales, SST variance is overestimated (underestimated) at periods between 5 and 10 ($>$10) years. Comparison of spectra at individual grid points reveals that the discrepancy at periods $>$ 10 years is not uniform throughout the domain, but primarily dominated by underestimates within the western Sargasso Sea and south of the Grand Banks that overpower overestimates along the Gulf Stream (not shown). These are regions where we expect a dominant role for horizontal advection, and their collocation with poorer stochastic model performance emphasizes how entrainment alone is insufficient to fully characterize SST behavior in this region (Figs. 7b,e).

The importance of ocean dynamics beyond entrainment becomes increasingly apparent in the STGe. Rebounds in SST autocorrelation associated with re-emergence are inconsistent with the behavior in CESM-FULL (Fig. 7c). Additionally, entrainment-related damping widens the disagreement with CESM-FULL, as the variance is underestimated at periods between 3 and 8 years (Fig. 7f), even if ENSO is removed from CESM-FULL (not shown). This suggests that missing processes from the stochastic model obscure the signal of reemergence and counteract entrainment-related damping of SST variability. One likely candidate is the subduction of anomalies in the seasonal thermocline into the ocean interior (Qiu and Huang 1995; Liu and Huang 2012), which may explain the similar lack of SST reemergence observed in this region (de Coëtlogon and Frankignoul 2003; Hanawa and Sugimoto 2004).

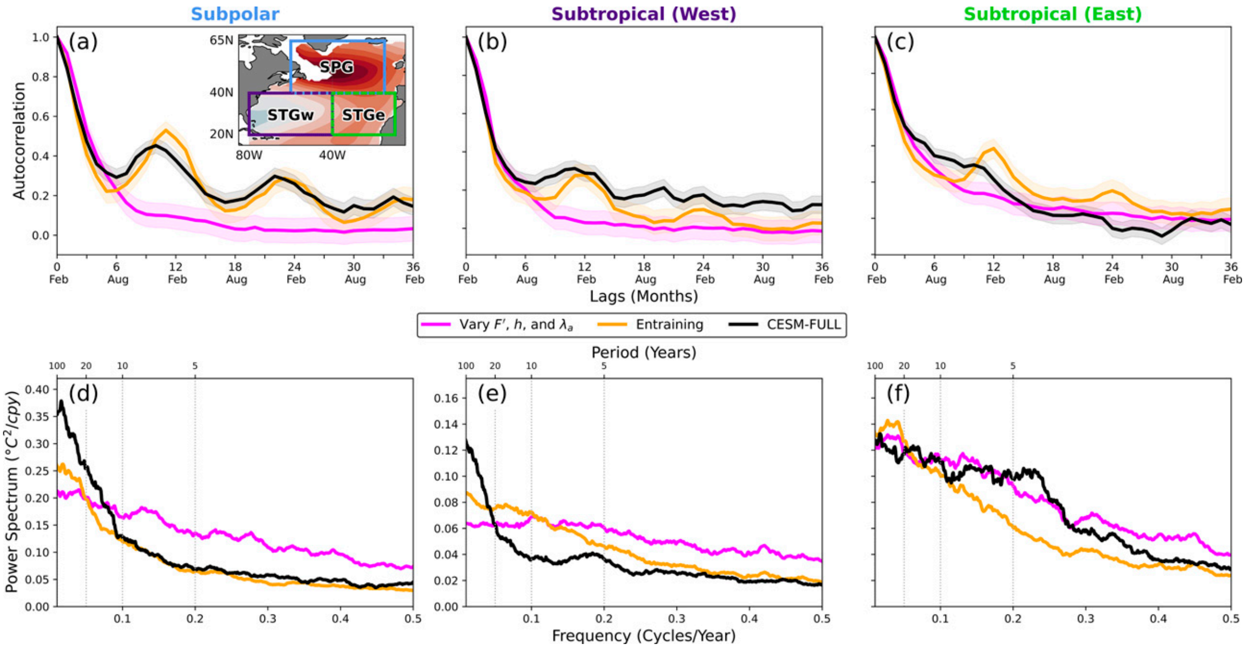

FIG. 7. The (a)–(c) autocorrelations and (d)–(f) power spectra for SST anomalies averaged over (a),(d) the SPG, and the subtropical gyre (b),(e) west and (c),(f) east. The corresponding bounding boxes are shown in the inset of (a), over the AMV pattern from CESM-SLAB. The colors corresponding to each model configuration (Level 4 Vary h and Level 5 Entraining) are identical to previous figures.

c. The AMV pattern

In this section, we investigate the ability of the stochastic model to reproduce the AMV pattern. We define the *extratropical* AMV index as the 10-yr low-pass filtered, area-weighted average of SST anomalies in 20°–60°N, 80°–0°W (section 4c). Including tropical points more than doubles the maximum AMV amplitude in the tropical Atlantic, but does not impact our conclusions (not shown). The AMV index is normalized and regressed back to the SST anomalies to obtain the AMV pattern (°C$\sigma_{\mathrm{AMV}}^{-1}$), representing the SST anomalies associated with typical AMV fluctuations (one standard deviation).

The stochastic model largely captures the spatial characteristics of AMV and its canonical horseshoe pattern (Fig. 8). Key features of CESM-SLAB pattern, including the maximum loading in the subpolar and tropical regions as well as the connection, albeit weaker, between the two centers along the eastern subtropics, are reproduced by the non-entraining stochastic model (Level 3 Vary F', λ_a)—the level of hierarchy that corresponds best to CESM-SLAB (Fig. 8a versus Fig. 8c). Despite capturing the general features of the AMV pattern, the amplitude of its centers of action and the AMV index remain underestimated: the variance of the index in the non-entraining model is 43% of CESM-SLAB (cf. Figs. 8a and 8c). A possible source for this discrepancy is the absence of two-way, air–sea feedbacks, such as the wind–evaporation–SST (WES) feedback, which may potentially enhance low-frequency variability (Oelsmann et al. 2020).

The SST maximum in CESM-FULL AMV pattern is weaker than in CESM-SLAB and shifted eastward, away from the sea ice edge, with no change of sign in the western subtropical gyre (cf. Figs. 8c and 8d). The variance of the AMV index in CESM-FULL is 45% of that in CESM-SLAB, reflecting enhanced low-frequency variability in the latter. This comparison underscores how the inclusion of ocean dynamics both alters the spatial pattern and damps its magnitude of variability (Murphy et al. 2021; Patrizio and Thompson 2021).

Including entrainment in the stochastic model (Level 5 Entraining) replicates this behavior by damping the pattern and shifting the subpolar maximum eastward, although too far toward regions of large annual MLD range in the northeast Atlantic (cf. Figs. 8a and 8b). This results in considerable underestimates in the amplitude of low-frequency variability: the entraining model's AMV index has 51% of the variance in CESM-FULL (cf. Figs. 8b and 8d). Thus, adding entrainment excessively damps SST, necessitating the inclusion of missing dynamics and nonlocal feedbacks, such as lateral advection or WES, to accurately represent the AMV amplitude and pattern.

Considering the importance of spatially coherent forcing in reproducing the AMV pattern, we explore if specific, leading modes of atmospheric variability play a dominant role. Originally, we forced the stochastic model by including enough EOF modes to explain 90% of the variance, with additional corrections to ensure a consistent amplitude. For this additional calculation, we force the stochastic model with only the first two EOFs of each month (which are the NAO and east Atlantic pattern (EAP), respectively), separately and in combination (i.e., EOF1 + EOF2), without variance correction. The first and second modes explain 26.47% and 17.02% of the F' variance, respectively. We focus our analysis on the entraining case (Level 5) for comparison to CESM-FULL.

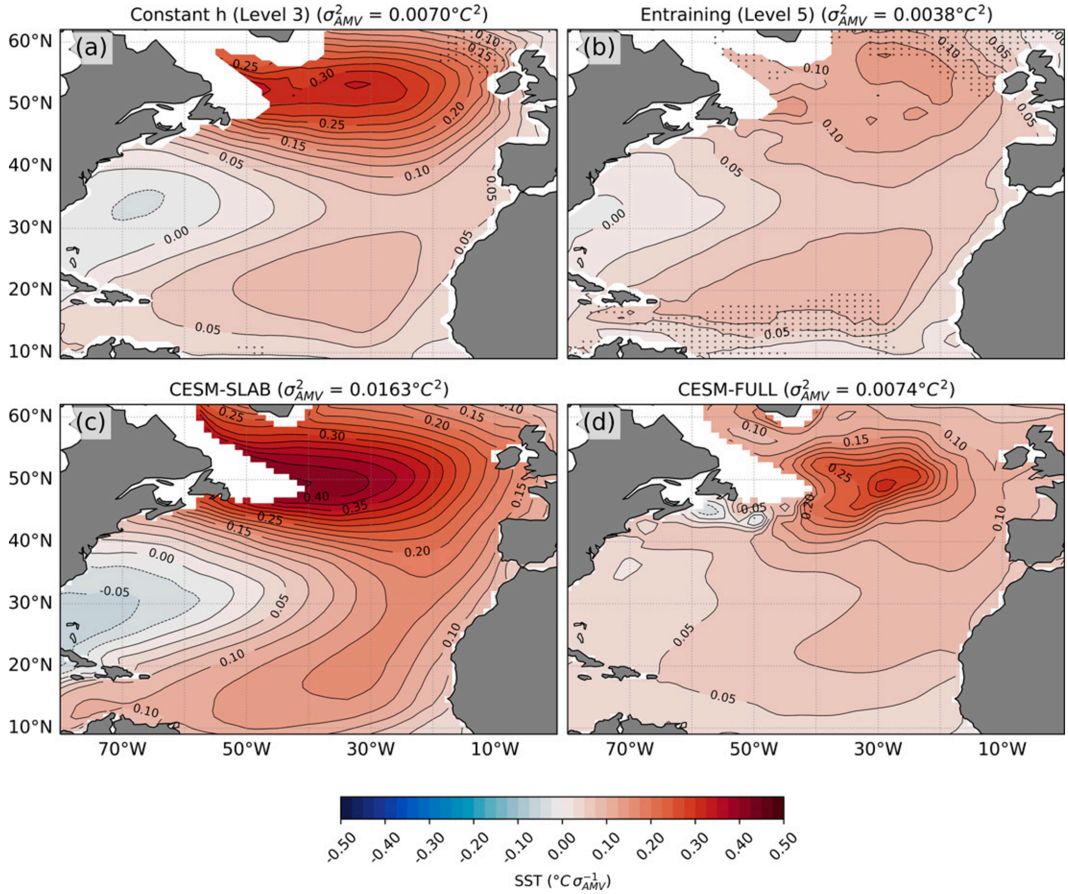

FIG. 8. Comparison of AMV patterns (contour interval = 0.025°C $\sigma^{-1}_{\mathrm{AMV}}$) from the stochastic models with (a) spatially varying, temporally constant h (i.e., non-entraining; Level 3 Vary F', λ_a) and (b) adding seasonally varying MLD and entrainment (Level 5 Entraining). The patterns from (c) CESM-SLAB and (d) CESM-FULL are also included. The variance of the AMV index for each case is indicated in the title. The stippled regions in (a) and (b) indicate where the estimated heat flux feedback is statistically insignificant, and is either set to 0 [in (a)] or replaced with the corresponding CESM-SLAB values [in (b)].

Forcing the stochastic model with dominant atmospheric modes alone, whether NAO-like or EAP-like, does not capture the canonical AMV pattern and underestimates its amplitude by an order of magnitude (Figs. 9a–c vs Figs. 8b,d). The first mode's pattern instead resembles the SST tripole with a negative pole in the subtropics, as expected from NAO forcing (Cayan 1992; Deser et al. 2010). Additionally, the northernmost maximum is displaced too far north (south) for EOF 1 (EOF 2) compared to the CESM-FULL AMV pattern. Applying both modes combined only slightly improves the comparison against CESM-FULL AMV pattern, but the negative subtropical pole persists. Therefore, the higher modes of atmospheric forcing are important for reproducing a single-signed AMV pattern across the basin.

6. Discussion

a. The role of ocean dynamics

While our analyses focus primarily on the contribution of seasonal variation and entrainment to AMV, several implications emerge for the broader role of ocean dynamics in SST variability. Prior to defining this role, we first qualify what falls under the umbrella of ocean dynamics by adopting one of two frameworks.

First, we consider the seasonal mixed-layer cycle and entrainment mechanism as part of the ocean's *local*, *passive* response as opposed to *nonlocal*, *active* ocean dynamics. Within this framework, our results suggest that active ocean dynamics are not essential for generating the *spatial pattern* of AMV. This agrees with Clement et al.'s (2015) statement that the AMV pattern arises from temporally stochastic atmospheric forcing, and further affirms the importance of spatial coherence in heat flux forcing. However, the stochastic model underestimates the *amplitude* of AMV relative to CESM1, leaving a role for the missing, active oceanic processes or nonlocal air–sea feedbacks.

A surprising result is the stochastic models' ability to reproduce the SST persistence and spectra in the SPG, a region where active ocean dynamics, such as overturning circulation and horizontal gyre circulation, are thought to play an important role in SST variability (McCarthy et al. 2015; Piecuch et al. 2017; Zhang 2017). Our results indicate that the collocated deep MLD and

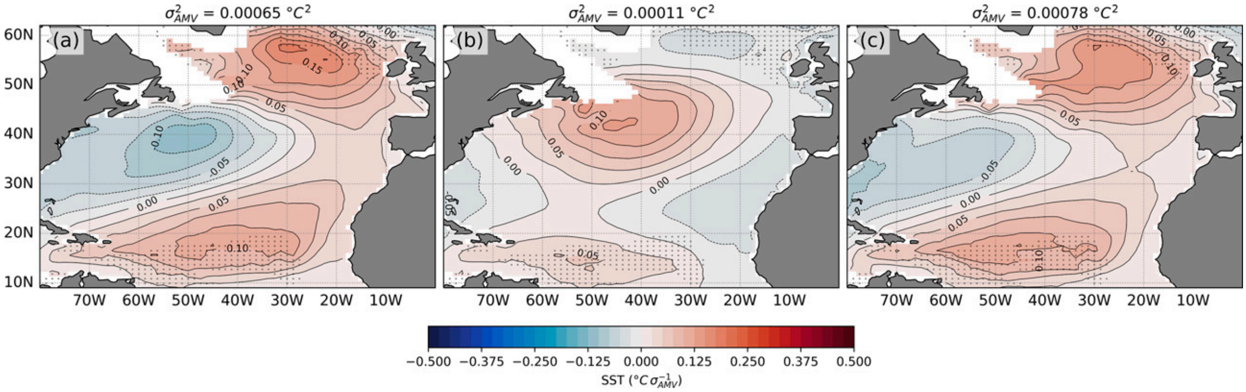

FIG. 9. The AMV patterns (°C $\sigma_{\rm AMV}^{-1}$) for the entraining stochastic model (Level 5) forced with (a) only EOF 1, (b) only EOF2, and (c) both EOFs of the CESM-FULL stochastic forcing (F'). The variance of the AMV index is indicated above each panel.

weak atmospheric damping synergistically enhance the memory of SST anomalies in the SPG (Fig. 2). This enhanced memory due to *local* conditions may explain the ability of slab simulations to produce multidecadal variability with spatiotemporal characteristics resembling AMV in the fully coupled system, but ultimately driven by different dynamical processes (Garuba et al. 2018; Oelsmann et al. 2020).

However, the SST and AMV variance in SLAB remain overestimated relative to FULL. Previous works have interpreted this difference as indicating the *net* damping effect of ocean dynamics (Yamamoto et al. 2020; Murphy et al. 2021; Patrizio and Thompson 2021). These are illustrative of a second framework, where all processes missing from SLAB, including seasonal MLD variation and entrainment, are subsumed under the umbrella of ocean dynamics. Our results support these previous assessments up to interannual time scales and suggest that entrainment is the primary damping mechanism rather than advection or nonlocal ocean dynamics. The stochastic model further reveals a frequency-dependent effect, where entrainment enhances (damps) variance at multidecadal (interannual) time scales over key AMV regions. Determination of the contribution of ocean dynamics for AMV is thus sensitive to the inclusion of entrainment and MLD variations.

Ratios of regionally averaged SST spectra underscore the importance of entrainment for understanding SLAB versus FULL differences and potential contributions of nonlocal ocean dynamics (Fig. 10). Previous works have described the greater variance of SST in SLAB simulations relative to both fully coupled models and observations, particularly at interannual time scales in the extratropical Atlantic (Zhang 2017; Garuba et al. 2018; Oelsmann et al. 2020; Murphy et al. 2021; Patrizio and Thompson 2021). A notable exception where both configurations have comparable power is found at periods > 50 years in STGw, suggesting a substantial contribution of ocean dynamics in this region (Fig. 10a). Unlike CESM-SLAB, the entraining stochastic model's spectra improve agreement with CESM-FULL, particularly at periods up to 20 years, highlighting the importance of including entrainment for representing SST behavior (Fig. 10b). A potential role of nonlocal ocean dynamics is suggested by the underestimates at periods > 20 years remains in the SPG and STGw. Further work is needed to identify the origin of additional of low-frequency variability, potentially through additionally levels in the stochastic model hierarchy that include nonlocal ocean processes.

b. *Uncertainties in parameter estimation*

Interpretation of our results should include clarification of uncertainties in parameter estimation. We estimated stochastic model parameters from CESM1, with the objective of applying the hierarchy to understand the AMV in SLAB and FULL simulations of this particular model. Differences in the relative importance of these parameters across other models and observations may exist, particularly considering model biases present in CESM1. For example, CESM1 has multidecadal

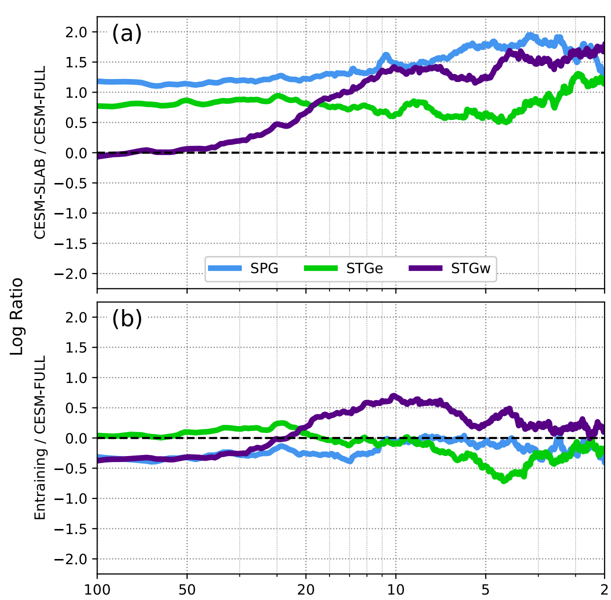

FIG. 10. The log ratio of regionally averaged SST spectra (a) between CESM-SLAB and FULL and (b) between the entraining stochastic model and CESM-FULL in the SPG, western subtropical gyre (STGw), and eastern subtropical gyre (STGe).

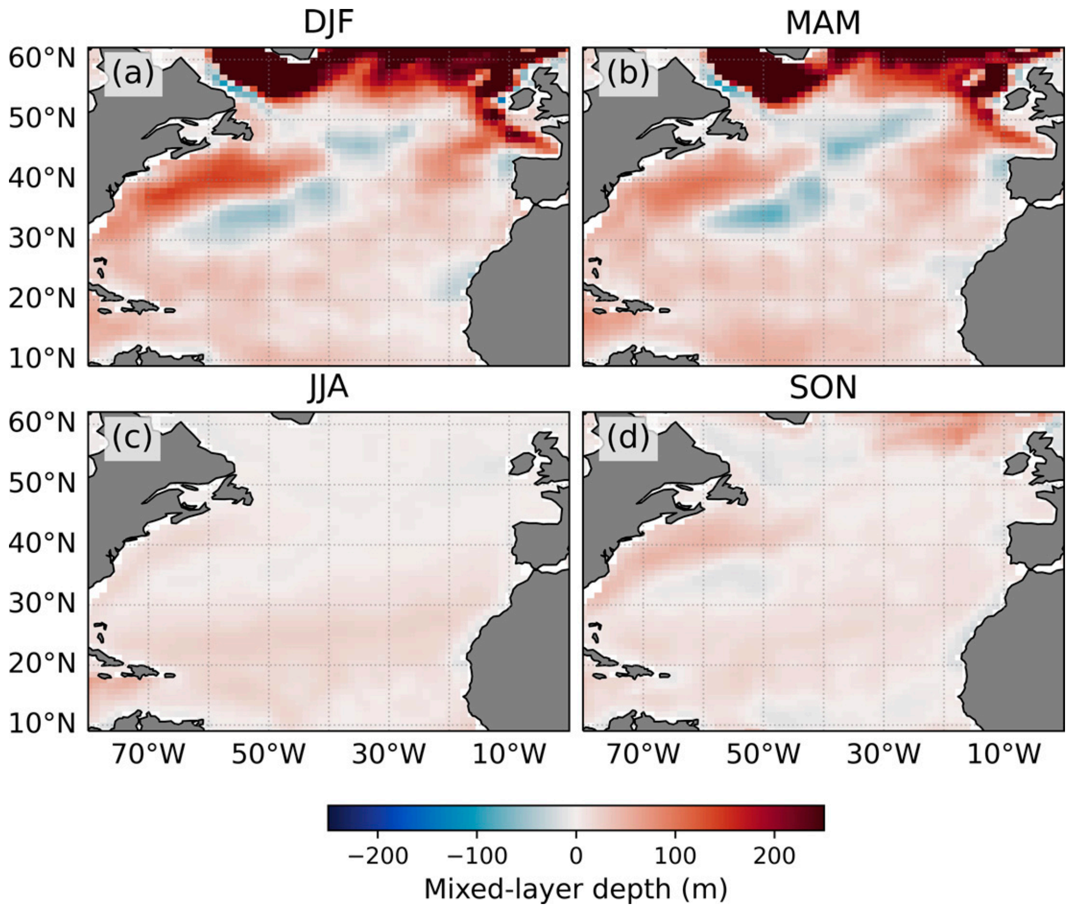

FIG. 11. Seasonal mean differences in MLD [CESM-FULL minus Monthly Isopycnal/Mixed-layer Ocean Climatology version 2.2 (MIMOC)], where positive values indicate overestimated MLD in CESM-FULL.

SST variability that is weaker than observations (Kim et al. 2018a; Murphy et al. 2021), indicating that the discrepancy in low-frequency SST variance between the entraining stochastic model and observations is greater than with CESM-FULL. Assuming that the AMV in the limited observational record is robust, our results suggest that either the representation of entrainment, forcing, and damping processes in CESM-FULL is different from observations, or that additional oceanic processes are needed to enhance SST variance at low frequencies. Identifying the contributions of each source to this discrepancy would involve application of the stochastic model hierarchy to other models and observations, and is left to future work.

Considering the importance of the seasonal mixed-layer cycle for recovering realistic amplitudes of SST variability, we examine MLD biases in CESM1 relative to an observational estimate from the Monthly Isopycnal/Mixed-layer Ocean Climatology version 2.2 (MIMOC) (Schmidtko et al. 2013). The winter and spring MLD in CESM1 are largely overestimated around Greenland, north of 50°N (Fig. 11). A deeper bias increases the heat capacity of the mixed layer, weakening both forcing and damping, suggesting that both CESM1 and the stochastic model overestimate SST persistence in this region. In contrast, the shallow MLD bias in the interior of the SPG, a key area for the maxima of the AMV pattern, may potentially explain the lack of power at low frequencies in CESM1 relative to observations (Kim et al. 2018a; Murphy et al. 2021).

Of further relevance to the memory of SSTs is uncertainty in the heat flux feedback estimates. Low-frequency variability is sensitive to the strength of air–sea coupling, and fully coupled model simulations may have heat flux feedbacks that are too strong (Garuba et al. 2018). Our estimates of heat flux feedback in CESM-SLAB and FULL exhibit pronounced differences, where CESM-FULL has stronger damping over the SPG, leading to an underestimate of SST variance by the latter (Fig. 12). A possible explanation is the lack of interactive ocean advection in SLAB, which increases the local SST autocovariance in SLAB, or the denominator in the feedback estimates [Eq. (7)]. The resulting weaker heat flux feedback leads to unrealistically large SPG SSTs in CESM-SLAB. If we integrate the non-entraining stochastic model (Level 3) with FULL heat flux feedback values rather than those from SLAB, the AMV index variance is reduced by 25.7%, highlighting the sensitivity of AMV amplitude to heat flux feedback estimates (not shown).

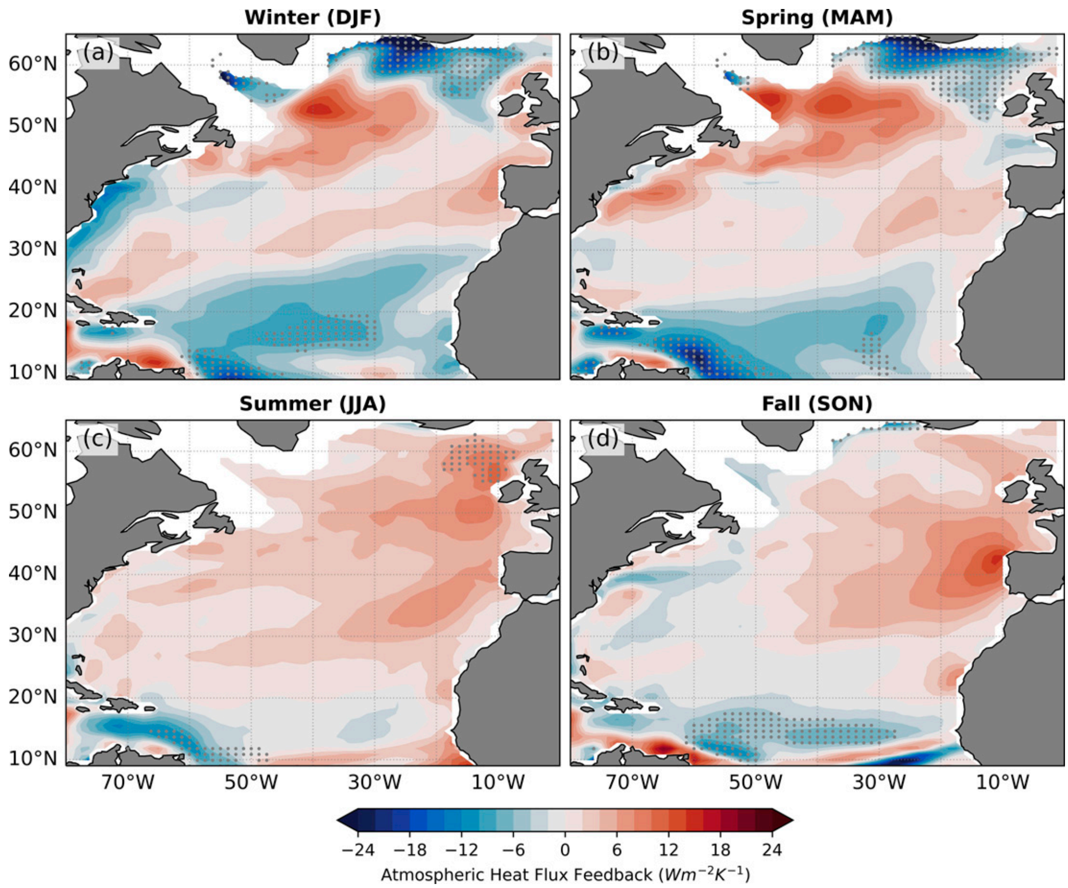

FIG. 12. Differences in seasonally averaged heat flux feedback between CESM-FULL and CESM-SLAB. Stippling indicates where either SLAB or FULL estimates are insignificant.

c. *Investigating additional ocean processes and limitations*

While comparisons between the entraining stochastic model and CESM-FULL provide a means to approximate the role of the missing ocean dynamics, further insight on individual processes can be obtained by revisiting the temperature equation [Eq. (1)] and investigating neglected terms or simplifying assumptions. An example is heat transport due to advection of the temperature gradient by anomalous Ekman currents [Eq. (1), term B], which can have magnitudes comparable to anomalous heat flux forcing but with different seasonal variation, reinforcing growth of extratropical Atlantic SST anomalies from late fall to early winter (Frankignoul and Reynolds 1983; Frankignoul 1985; Peng et al. 2006). Previous work has found that inclusion of Ekman forcing (Q_{ek}) is important for obtaining detailed structure and correct magnitude of large-scale SST patterns (Alexander and Scott 2008). For a preliminary attempt, we compute the advection of the mean temperature gradient due to anomalous Ekman currents vertically integrated to the mean climatological MLD:

$$Q_{ek} = -\frac{c_p}{f}\left(\tau_y \frac{\partial \overline{T}}{\partial x} - \tau_x \frac{\partial \overline{T}}{\partial y}\right), \tag{10}$$

where f is the Coriolis parameter and τ is the anomalous wind stress, obtained via regression to the PCs from our EOF analysis of F', thus recovering the seasonal patterns of wind stress related to dominant atmospheric modes. The term Q_{ek} is not applied at points adjacent to coastlines to focus on lateral effects rather than vertical upwelling (Alexander and Scott 2008). Since Q_{ek} depends on atmospheric variables with short memory, it is scaled by the same white noise time series as F' [see Eq. (8)].

The addition of Q_{ek} to the entraining model (Level 5+) leads to increases in low-frequency SST variance in the SPG (Fig. 13b), but degrades performance at higher frequencies and in other regions (Fig. 13c vs Fig. 10b). The most noticeable impact is on the AMV pattern: the subpolar maximum is enhanced and shifted southward toward the region with the largest SST gradient near the North Atlantic Current (Fig. 13a). This suggests that Q_{ek} is a potential source of additional low-frequency variability and slightly improves the ability of the stochastic model to capture the spatial aspects of AMV in the subpolar region.

An additional assumption to interrogate is the fixed seasonal cycle in MLD. Previous studies have noted that MLD anomalies, in concert with anomalous heat fluxes, act to warm the SPG region, playing an important role in modulating AMV

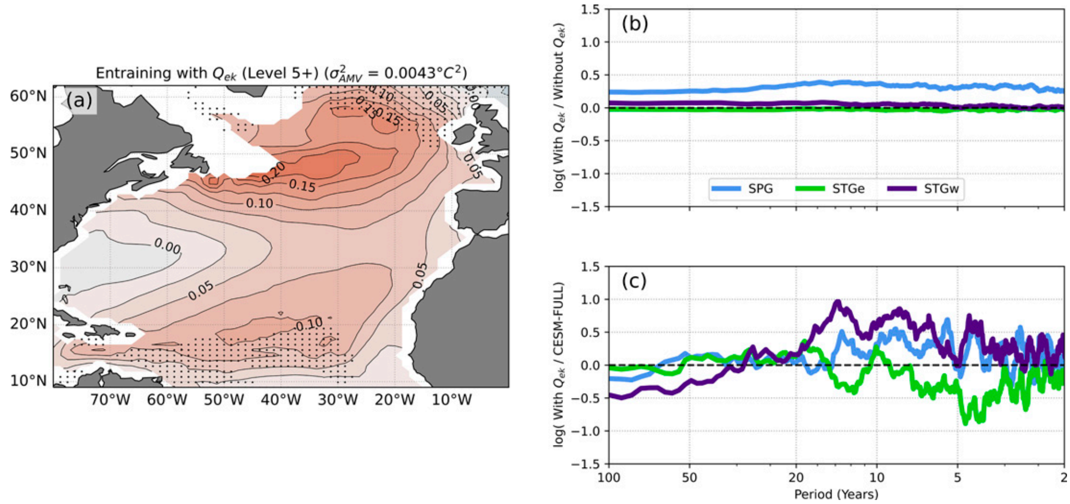

FIG. 13. (a) AMV pattern (contour interval = 0.025°C σ_{AMV}^{-1}) for the entraining stochastic model with Ekman forcing (Level 5+). Log ratios of regionally averaged SST spectra (b) between the entraining stochastic model with (Level 5+) and without (Level 5) Ekman forcing and (c) between the entraining stochastic model with Ekman forcing (Level 5+) with CESM-FULL.

(Yamamoto et al. 2020; Li et al. 2020). Interannual MLD variations could thus provide a source of enhanced variability at low frequencies, but could also impact the entrainment mechanism by preventing consistent re-emergence of wintertime anomalies, potentially reducing memory of wintertime SSTs (Buckley et al. 2019). Critical examination of MLD variability's competing effects on the memory of SST anomalies is needed to constrain its impact on AMV.

As a low-resolution model, CESM1 has limitations in representations of ocean processes, such as biases in the Gulf Stream position and separation and reduced variance due to lack of eddies, as commonly found in other low-resolution climate models (Kirtman et al. 2012). Since the parameters of the stochastic model and inferred role of the ocean dynamics beyond entrainment depend upon CESM1, our results are limited to understanding only SST variability and AMV within this model. Further work involving analysis of higher-resolution models or observations is needed to discern the role of ocean processes misrepresented in CESM1. In addition to resolution dependence, repeating the study for other models can serve to evaluate intermodal consistency in the role of entrainment.

7. Summary

Studies partitioning ocean–atmosphere contributions to AMV employ comparisons between model simulations with slab and fully dynamic ocean components. However, complete removal of interactive ocean dynamics in slab-like configurations prevents transparent understanding of how individual processes contribute to SST variability and SLAB-FULL differences. We use a hierarchy of stochastic models to systematically investigate the contribution of seasonal variation in upper-ocean parameters and mixed-layer entrainment in SLAB and FULL CESM1 simulations.

The entraining stochastic model successfully reproduced both the seasonal persistence and SST spectra at the subpolar maximum of the CESM-FULL AMV pattern. We expanded our analysis to key regions of the AMV pattern in the North Atlantic to isolate the role of entrainment and its ability to reproduce regional autocorrelation, spectra, and AMV pattern compared to the corresponding CESM simulation. The key findings of this work are as follows:

1) Seasonal variation in atmospheric forcing and upper-ocean parameters is important for capturing SST behavior, and the absence of seasonal MLD variations in CESM-SLAB creates unrealistic persistence and enhanced low-frequency variance.
2) Entrainment damps SSTs at interannual time scales, but slightly enhances variance at decadal and longer time scales when considering area-averaged SST over key extratropical regions of the AMV pattern. The variance at low frequencies remains underestimated, leaving a role for missing nonlocal feedbacks or ocean dynamics, such as advection or subduction (section 3a), to enhance SST variability.
3) The canonical AMV horseshoe pattern is reproduced by spatially coherent stochastic atmospheric forcing, but its amplitude is underestimated by up to ~50%, suggesting that two-way large-scale air–sea coupling, and/or ocean dynamics substantially contribute to AMV.

To conclude, we emphasize that the objective of the stochastic model hierarchy is not the perfect simulation of SSTs, but to improve physical understanding of how individual processes contribute to SST variability. Our investigation elucidated the importance of both seasonal variation and entrainment for capturing the persistence and spectra of SST and understanding the SLAB versus FULL variance difference. Comparison with CESM-FULL suggests that ocean dynamics absent from the stochastic model play a substantial role in capturing the amplitude of SST variability, particularly at low frequencies and over regions such as the western subtropics. Thus, delineating the ocean's role for AMV requires careful consideration of both mixed-layer depth variations and entrainment and further investigation of individual ocean processes.

Acknowledgments. The authors gratefully acknowledge support from the U.S. Department of Energy Office of Science Biological and Environmental Research as part of the Regional and Global Model Analysis program area (DE-SC0019492). GL is supported by the Department of Defense (DoD) through the National Defense Science and Engineering Graduate (NDSEG) Fellowship Program. The authors are also very grateful to three anonymous reviewers and the editor Dr. Robert Wills for their thorough and insightful comments.

Data availability statement. All data used for this work are available online. CESM1 Pre-industrial control simulations are available through the NCAR Climate Data Gateway (https://www.cesm.ucar.edu/projects/community-projects/LENS/data-sets.html). MIMOC is available through https://www.pmel.noaa.gov/mimoc/.

REFERENCES

Alexander, M. A., and C. Deser, 1995: A mechanism for the recurrence of wintertime midlatitude SST anomalies. *J. Phys. Oceanogr.*, **25**, 122–137, https://doi.org/10.1175/1520-0485(1995)025<0122:AMFTRO>2.0.CO;2.

——, and C. Penland, 1996: Variability in a mixed layer ocean model driven by stochastic atmospheric forcing. *J. Climate*, **9**, 2424–2442, https://doi.org/10.1175/1520-0442(1996)009<2424:VIAMLO>2.0.CO;2.

——, and J. D. Scott, 2008: The role of Ekman ocean heat transport in the Northern Hemisphere response to ENSO. *J. Climate*, **21**, 5688–5707, https://doi.org/10.1175/2008JCLI2382.1.

Alheit, J., P. Licandro, S. Coombs, A. Garcia, A. Giráldez, M. T. G. Santamaría, A. Slotte, and A. C. Tsikliras, 2014: Reprint of "Atlantic Multidecadal Oscillation (AMO) modulates dynamics of small pelagic fishes and ecosystem regime shifts in the eastern North and Central Atlantic". *J. Mar. Syst.*, **133**, 88–102, https://doi.org/10.1016/j.jmarsys.2014.02.005.

Bitz, C. M., K. M. Shell, P. R. Gent, D. A. Bailey, G. Danabasoglu, K. C. Armour, M. M. Holland, and J. T. Kiehl, 2012: Climate sensitivity of the Community Climate System Model, version 4. *J. Climate*, **25**, 3053–3070, https://doi.org/10.1175/JCLI-D-11-00290.1.

Buckley, M. W., T. DelSole, M. S. Lozier, and L. Li, 2019: Predictability of North Atlantic sea surface temperature and upper-ocean heat content. *J. Climate*, **32**, 3005–3023, https://doi.org/10.1175/JCLI-D-18-0509.1.

Byju, P., D. Dommenget, and M. A. Alexander, 2018: Widespread reemergence of sea surface temperature anomalies in the global oceans, including tropical regions forced by reemerging winds. *Geophys. Res. Lett.*, **45 (15)**, 7683–7691, https://doi.org/10.1029/2018GL079137.

Cayan, D. R., 1992: Latent and sensible heat flux anomalies over the northern oceans: Driving the sea surface temperature. *J. Phys. Oceanogr.*, **22**, 859–881, https://doi.org/10.1175/1520-0485(1992)022<0859:LASHFA>2.0.CO;2.

Clement, A., P. DiNezio, and C. Deser, 2011: Rethinking the ocean's role in the southern oscillation. *J. Climate*, **24**, 4056–4072, https://doi.org/10.1175/2011JCLI3973.1.

——, K. Bellomo, L. N. Murphy, M. A. Cane, T. Mauritsen, G. Rädel, and B. Stevens, 2015: The Atlantic multidecadal oscillation without a role for ocean circulation. *Science*, **350**, 320–324, https://doi.org/10.1126/science.aab3980.

Davis, R. E., R. deSzoeke, and P. Niiler, 1981: Variability in the upper ocean during MILE. Part II: Modeling the mixed layer response. *Deep-Sea Res.*, **28A**, 1453–1475, https://doi.org/10.1016/0198-0149(81)90092-3.

de Coëtlogon, G., and C. Frankignoul, 2003: The persistence of winter sea surface temperature in the North Atlantic. *J. Climate*, **16**, 1364–1377, https://doi.org/10.1175/1520-0442-16.9.1364.

Deser, C., M. A. Alexander, and M. S. Timlin, 2003: Understanding the persistence of sea surface temperature anomalies in midlatitudes. *J. Climate*, **16**, 57–72, https://doi.org/10.1175/1520-0442(2003)016<0057:UTPOSS>2.0.CO;2.

——, ——, S.-P. Xie, and A. S. Phillips, 2010: Sea surface temperature variability: Patterns and mechanisms. *Annu. Rev. Mar. Sci.*, **2**, 115–143, https://doi.org/10.1146/annurev-marine-120408-151453.

Frankignoul, C., 1985: Sea surface temperature anomalies, planetary waves, and air–sea feedback in the middle latitudes. *Rev. Geophys.*, **23**, 357–390, https://doi.org/10.1029/RG023i004p00357.

——, and K. Hasselmann, 1977: Stochastic climate models, Part II: Application to sea-surface temperature anomalies and thermocline variability. *Tellus*, **29**, 289–305, https://doi.org/10.3402/tellusa.v29i4.11362.

——, and R. W. Reynolds, 1983: Testing a dynamical model for midlatitude sea surface temperature anomalies. *J. Phys. Oceanogr.*, **13**, 1131–1145, https://doi.org/10.1175/1520-0485(1983)013<1131:TADMFM>2.0.CO;2.

——, and E. Kestenare, 2002: The surface heat flux feedback. Part I: Estimates from observations in the Atlantic and the North Pacific. *Climate Dyn.*, **19**, 633–647, https://doi.org/10.1007/s00382-002-0252-x.

——, A. Czaja, and B. L'Heveder, 1998: Air–sea feedback in the North Atlantic and surface boundary conditions for ocean models. *J. Climate*, **11**, 2310–2324, https://doi.org/10.1175/1520-0442(1998)011<2310:ASFITN>2.0.CO;2.

Gao, M., J. Yang, D. Gong, P. Shi, Z. Han, and S.-J. Kim, 2019: Footprints of Atlantic multi-decadal oscillation in the low-frequency variation of extreme high temperature in the Northern Hemisphere. *J. Climate*, **32**, 791–802, https://doi.org/10.1175/JCLI-D-18-0446.1.

Garuba, O. A., J. Lu, H. A. Singh, F. Liu, and P. Rasch, 2018: On the relative roles of the atmosphere and ocean in the Atlantic multidecadal variability. *Geophys. Res. Lett.*, **45**, 9186–9196, https://doi.org/10.1029/2018GL078882.

Hanawa, K., and S. Sugimoto, 2004: 'Reemergence' areas of Winter Sea surface temperature anomalies in the world's oceans. *Geophys. Res. Lett.*, **31**, L10303, https://doi.org/10.1029/2004GL019904.

Hasselmann, K., 1976: Stochastic climate models Part I. Theory. *Tellus*, **28**, 473–485, https://doi.org/10.1111/j.2153-3490.1976.tb00696.x.

He, J., C. Deser, and B. J. Soden, 2017: Atmospheric and oceanic origins of tropical precipitation variability. *J. Climate*, **30**, 3197–3217, https://doi.org/10.1175/JCLI-D-16-0714.1.

Hosoda, S., M. Nonaka, T. Tomita, B. Taguchi, H. Tomita, and N. Iwasaka, 2016: Impact of downward heat penetration below the shallow seasonal thermocline on the sea surface temperature. *"Hot Spots" in the Climate System*, H. Nakamura et al., Eds., Springer, 73–89.

Hurrell, J. W., and Coauthors, 2013: The Community Earth System Model: A framework for collaborative research. *Bull. Amer. Meteor. Soc.*, **94**, 1339–1360, https://doi.org/10.1175/BAMS-D-12-00121.1.

Kim, W. M., S. Yeager, P. Chang, and G. Danabasoglu, 2018a: Low-frequency North Atlantic climate variability in the Community Earth System Model large ensemble. *J. Climate*, **31**, 787–813, https://doi.org/10.1175/JCLI-D-17-0193.1.

——, S. G. Yeager, and G. Danabasoglu, 2018b: Key role of internal ocean dynamics in Atlantic multidecadal variability during the last half century. *Geophys. Res. Lett.*, **45**, 13 449–13 457, https://doi.org/10.1029/2018GL080474.

Kirtman, B. P., and Coauthors, 2012: Impact of ocean model resolution on CCSM climate simulations. *Climate Dyn.*, **39**, 1303–1328, https://doi.org/10.1007/s00382-012-1500-3.

Knight, J. R., R. J. Allan, C. K. Folland, M. Vellinga, and M. E. Mann, 2005: A signature of persistent natural thermohaline circulation cycles in observed climate. *Geophys. Res. Lett.*, **32**, L20708, https://doi.org/10.1029/2005GL024233.

Li, L., M. S. Lozier, and M. W. Buckley, 2020: An investigation of the ocean's role in Atlantic multidecadal variability. *J. Climate*, **33**, 3019–3035, https://doi.org/10.1175/JCLI-D-19-0236.1.

Liu, L. L., and R. X. Huang, 2012: The global subduction/obduction rates: Their interannual and decadal variability. *J. Climate*, **25**, 1096–1115, https://doi.org/10.1175/2011JCLI4228.1.

McCarthy, G. D., I. D. Haigh, J. J.-M. Hirschi, J. P. Grist, and D. A. Smeed, 2015: Ocean impact on decadal Atlantic climate variability revealed by sea-level observations. *Nature*, **521**, 508–510, https://doi.org/10.1038/nature14491.

Meehl, G. A., and Coauthors, 2021: Atlantic and Pacific tropics connected by mutually interactive decadal-timescale processes. *Nat. Geosci.*, **14**, 36–42, https://doi.org/10.1038/s41561-020-00669-x.

Murphy, L. N., J. M. Klavans, A. C. Clement, and M. A. Cane, 2021: Investigating the roles of external forcing and ocean circulation on the Atlantic multidecadal SST variability in a large ensemble climate model hierarchy. *J. Climate*, **34**, 4835–4849, https://doi.org/10.1175/JCLI-D-20-0167.1.

Oelsmann, J., L. Borchert, R. Hand, J. Baehr, and J. H. Jungclaus, 2020: Linking ocean forcing and atmospheric interactions to Atlantic multidecadal variability in MPI-ESM1.2. *Geophys. Res. Lett.*, **47**, e2020GL087259, https://doi.org/10.1029/2020GL087259.

O'Reilly, C. H., M. Huber, T. Woollings, and L. Zanna, 2016: The signature of low-frequency oceanic forcing in the Atlantic multidecadal oscillation. *Geophys. Res. Lett.*, **43**, 2810–2818, https://doi.org/10.1002/2016GL067925.

Ortiz, M. J., and A. R. de Elvira, 1985: A cyclo-stationary model of sea surface temperatures in the Pacific Ocean. *Tellus*, **37A**, 14–23, https://doi.org/10.3402/tellusa.v37i1.11651.

Park, S., C. Deser, and M. A. Alexander, 2005: Estimation of the surface heat flux response to sea surface temperature anomalies over the global oceans. *J. Climate*, **18**, 4582–4599, https://doi.org/10.1175/JCLI3521.1.

——, M. A. Alexander, and C. Deser, 2006: The impact of cloud radiative feedback, remote ENSO forcing, and entrainment on the persistence of North Pacific sea surface temperature anomalies. *J. Climate*, **19**, 6243–6261, https://doi.org/10.1175/JCLI3957.1.

Patrizio, C. R., and D. W. Thompson, 2021: Quantifying the role of ocean dynamics in ocean mixed layer temperature variability. *J. Climate*, **34**, 2567–2589, https://doi.org/10.1175/JCLI-D-20-0476.1.

——, and ——, 2022: Understanding the role of ocean dynamics in mid-latitude sea surface temperature variability using a simple stochastic climate model. *J. Climate*, **35**, 3313–3333, https://doi.org/10.1175/JCLI-D-21-0184.1.

Peng, S., W. A. Robinson, S. Li, and M. A. Alexander, 2006: Effects of Ekman transport on the NAO response to a tropical Atlantic SST anomaly. *J. Climate*, **19**, 4803–4818, https://doi.org/10.1175/JCLI3910.1.

Piecuch, C. G., R. M. Ponte, C. M. Little, M. W. Buckley, and I. Fukumori, 2017: Mechanisms underlying recent decadal changes in subpolar North Atlantic Ocean heat content. *J. Geophys. Res. Oceans*, **122**, 7181–7197, https://doi.org/10.1002/2017JC012845.

Qiu, B., and R. X. Huang, 1995: Ventilation of the North Atlantic and North Pacific: Subduction versus obduction. *J. Phys. Oceanogr.*, **25**, 2374–2390, https://doi.org/10.1175/1520-0485(1995)025<2374:VOTNAA>2.0.CO;2.

Schmidtko, S., G. C. Johnson, and J. M. Lyman, 2013: MIMOC: A global monthly isopycnal upper-ocean climatology with mixed layers. *J. Geophys. Res. Oceans*, **118**, 1658–1672, https://doi.org/10.1002/jgrc.20122.

Smith, R., and Coauthors, 2010: The Parallel Ocean Program (POP) reference manual, ocean component of the Community Climate System Model (CCSM) and Community Earth System Model (CESM). Tech. Rep. LAUR-10-01853, LANL, 141 pp., https://www.cesm.ucar.edu/models/cesm1.0/pop2/doc/sci/POPRefManual.pdf.

Yamamoto, A., H. Tatebe, and M. Nonaka, 2020: On the emergence of the Atlantic multidecadal SST signal: A key role of the mixed layer depth variability driven by North Atlantic oscillation. *J. Climate*, **33**, 3511–3531, https://doi.org/10.1175/JCLI-D-19-0283.1.

Zhang, R., and T. L. Delworth, 2006: Impact of Atlantic multidecadal oscillations on India/Sahel rainfall and Atlantic hurricanes. *Geophys. Res. Lett.*, **33**, L17712, https://doi.org/10.1029/2006GL026267.

——, 2017: On the persistence and coherence of subpolar sea surface temperature and salinity anomalies associated with the atlantic multidecadal variability. *Geophys. Res. Lett.*, **44 (15)**, 7865–7875, https://doi.org/10.1002/2017GL074342.

——, R. Sutton, G. Danabasoglu, T. L. Delworth, W. M. Kim, J. Robson, and S. G. Yeager, 2016: Comment on "The Atlantic multidecadal oscillation without a role for ocean circulation." *Science*, **352**, 1527, https://doi.org/10.1126/science.aaf1660.

——, ——, ——, Y.-O. Kwon, R. Marsh, S. G. Yeager, D. E. Amrhein, and C. M. Little, 2019: A review of the role of the Atlantic meridional overturning circulation in Atlantic multidecadal variability and associated climate impacts. *Rev. Geophys.*, **57**, 316–375, https://doi.org/10.1029/2019RG000644.